INTERNATIONAL JOURNAL OF PRECISION ENGINEERING AND MANUFACTURING Vol. 19, No. 1, pp. 109-118 JANUARY 2018 / 109

REGULAR PAPER

DOI: 10.1007/s12541-018-0013-3
ISSN 2234-7593 (Print) / 2005-4602 (Online)

Design and Testing of a New 3-DOF Spatial Flexure Parallel Micropositioning Stage

Xiaozhi Zhang[1] and Qingsong Xu[1,#]

1 Department of Electromechanical Engineering, Faculty of Science and Technology, University of Macau, Avenida da Universidade, Taipa, Macau, 999078, China
Corresponding Author / E-mail: qsxu@umac.mo, TEL: +853-8822-4278

KEYWORDS: Spatial flexure hinges, Compound displacement amplifier, 3-DOF parallel mechanism, Micropositioning stage

This paper presents the design and testing of a novel 3-DOF parallel flexure micropositioning stage for micro-scale operations. The proposed modular design can obtain the merit of high interchangeability during maintenance process. The output platform of the mechanism offers pure translational motion along X, Y, and Z axes by resorting to the flexure guiding of two parallelogram joints. Meanwhile, the output motion is decoupled by using two leaves with symmetric ellipse-shaped flexure hinges, and the platform provides isolated movement without parasitic motion. By using the bridge-type and lever-type compound amplifier, the micropositioning stage provides a large output displacement, which is over 30 times the input displacement provided by piezoelectric actuator. The enlarged displacement is translated to the orthogonal parallel mechanism by four straight beams, which provide perfect decoupling properties. In addition, the modular design principle makes it possible to adopt multiple materials to balance the performance of the actuator and decoupling flexure hinges. Analytical analysis and finite element analysis simulation are conducted to verify the fine decoupling property and large translational motion of the proposed 3-DOF parallel micropositioning stage. Moreover, a prototype is fabricated using multiple materials for experimental testing. Results demonstrate the promising performance of the developed decoupled micropositioning stage.

Manuscript received: February 19, 2017 / Revised: June 13, 2017 / Accepted: September 8, 2017

1. Introduction

Micro/nano-positioning technology has become an important approach for the applications which demand the merits of high accuracy and fast response. Micropositioning stages exhibit comprehensive applications not only in modern precision robotic research, such as robot arms of bionic handling assistant[1] and selective compliance assembly,[2] but also in industry such as high-speed pick-and-place operation,[3] high-resolution manufacturing[4] and assembly[5] in micro/nano-meter scale. It has also been combined with microgripper dedicated to high-precision positioning tasks, such as manipulating biological cells.[6]

In consideration of the high-resolution requirement, the stages are usually actuated by motors such as stack piezoelectric actuators (PZTs), voice coil motors (VCMs), magnetic levitation motors, and so on.[7] In particular, the PZT obtains the merits of rapid response, ultrahigh displacement resolution, and large output stiffness. However, the limited output stroke in micrometer level and the hysteresis nonlinearity effect block the wide applications of PZTs. While the hysteresis effect can be compensated by resorting to appropriate control technique, the limited stroke has to be resolved by mechanical design approach. To overcome the disadvantage of limited stroke, the lever-type displacement amplifier with flexure hinge is usually employed in the literature.[8] Another method to cope with the limited output is to insert a PZT into a bridge-type amplifier, which has been widely applied in recent research. For instance, the work[9] presents a lever-principle amplification micro-mechanism by merging smart material and micro-electromechanical system to obtain an amplification ratio of 5.48. The analytical model for a bridge-type amplifier is proposed by Ref. 10 based on elastic theory, and finite element method is applied to compare the mathematical model and simulation results for the model analysis. In addition, a detailed analysis of the bridge-type amplifier is reported in Ref. 11 based on stiffness modeling and geometry relationships. Later, a specific analysis is presented in Ref. 12, which provides a theoretical displacement amplification formula and obtains an amplification ratio of about 7.5. More recent works on bridge-type amplifiers can be found in the literature.[13,14]

Regarding the kinematic schemes, the micropositioning stages can be classified into two types in terms of serial kinematics and parallel

kinematics. Although the serial-kinematics structure can realize a compact design,[15] the accumulated error and parasitic motion are the main shortcoming in serial stages. As compared with serial micropositioning stage, the parallel-kinematics stage can achieve higher precision and faster response. Moreover, the parallel stage can obtain decoupled output motion and almost identical dynamics performance in each working direction.[16,17] Majority of current works are focused on planar micropositioning stage design.[18-23] Relatively fewer works on spatial micropositioning stages have been carried out.[24] Recently, a spatial positioner is proposed in Ref. 25, which obtains the combined rotational and translational output motion using a 3-PRS compliant parallel mechanism. A modified 6-PSS parallel mechanism-based micropositioning stage is designed in Ref. 26 for adjusting optical element. For some applications, such as biological cell microinjection, a 3-DOF stage with translational motion is sufficient. A few of orthogonal and non-orthogonal 3-DOF translational flexure parallel stages have been developed in the literature.[7,27-29]

As compared with non-orthogonal positioner, the orthogonal positioner can be easily controlled, but the cross-axis motion is a complex problem to handle. In addition, the orthogonal positioner can accommodate the large size of bridge-type amplifier. However, it is challenge to design a decoupled compliant parallel stage with both a compact size and a large workspace. To this end, a new orthogonal-type positioning stage is devised in this work. The overall size of the positioner mechanism is only 77 mm × 77 mm × 77 mm, which is much smaller than the recent design of XYZ stage[29] with the size of 105 mm × 105 mm × 105 mm.

The major contribution of this work is the design and testing of a novel compact XYZ micropositioning stage with large workspace and decoupled motion. In the following parts of the paper, the mechanical design is detailed in Section 2. Analytical models are derived in Section 3 and verified by conducting finite-element analysis (FEA) simulation study in Section 4. Section 5 presents the fabricated prototype and experimental studies. Concluding remarks are summarized in Section 6.

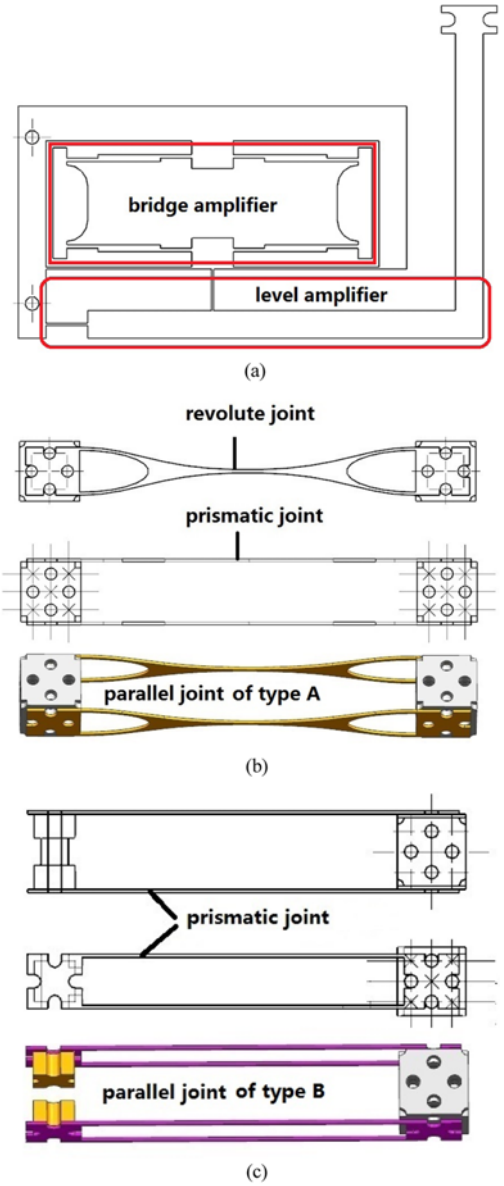

Fig. 1 Designed flexure mechanisms; Schematic diagram of (a) compound amplifier module, (b) decoupling flexure hinge module of type A, and (c) decoupling flexure hinge module of type B

2. Mechanical Design of the Parallel Positioner

In this section, the concept of modular design is first introduced in detail. Then, the assembly process of the parallel positioning stage is proposed.

2.1 Modular design

The modular design is widely applied in industry engineering, especially in quantity production owing to the advantages of high productive efficiency and easy to be repaired. To enable a decoupled parallel positioning motion, the proposed module needs to offer unique properties such as decoupling, motion guiding, etc. So, the designed positioner is divided into the modules of compound amplifier, flexure hinge, and PZT.

Although the selected PZT actuator (model P-885.91 from PI GmbH) provides larger output force, faster response and larger output stroke relative to other types, the limited output stroke of PZT actuator is still a demerit. Hence, the module of compound amplifier is proposed to overcome the limited stroke of the PZT actuator. As shown in Fig. 1(a), the compound amplifier is constructed with the combination of the lever-principle amplifier and bridge-principle amplifier, which is used to obtain a larger travel stroke along the working direction.

Concerning a decoupled parallel-kinematic mechanism, the key point is to alleviate the cross-axis motion. The parallel flexure hinges can be used to solve this problem perfectly. For example, the flexure hinges as shown in Fig. 1(b) have two pairs of prismatic (P) joint with leaf decoupling flexure hinges and revolute (R) joints with ellipse-shaped decoupling flexure hinges. They are termed parallel joint of type A, which consists of a pair of ellipse-shaped decoupling flexure hinges. They are used to decouple the two-dimensional cross-axis motion between the amplifier module and output platform. As shown in Fig. 1(c), two pairs of double prismatic joints, which are termed parallel joint of leaf flexure (type B), can cancel the cross-axis motion

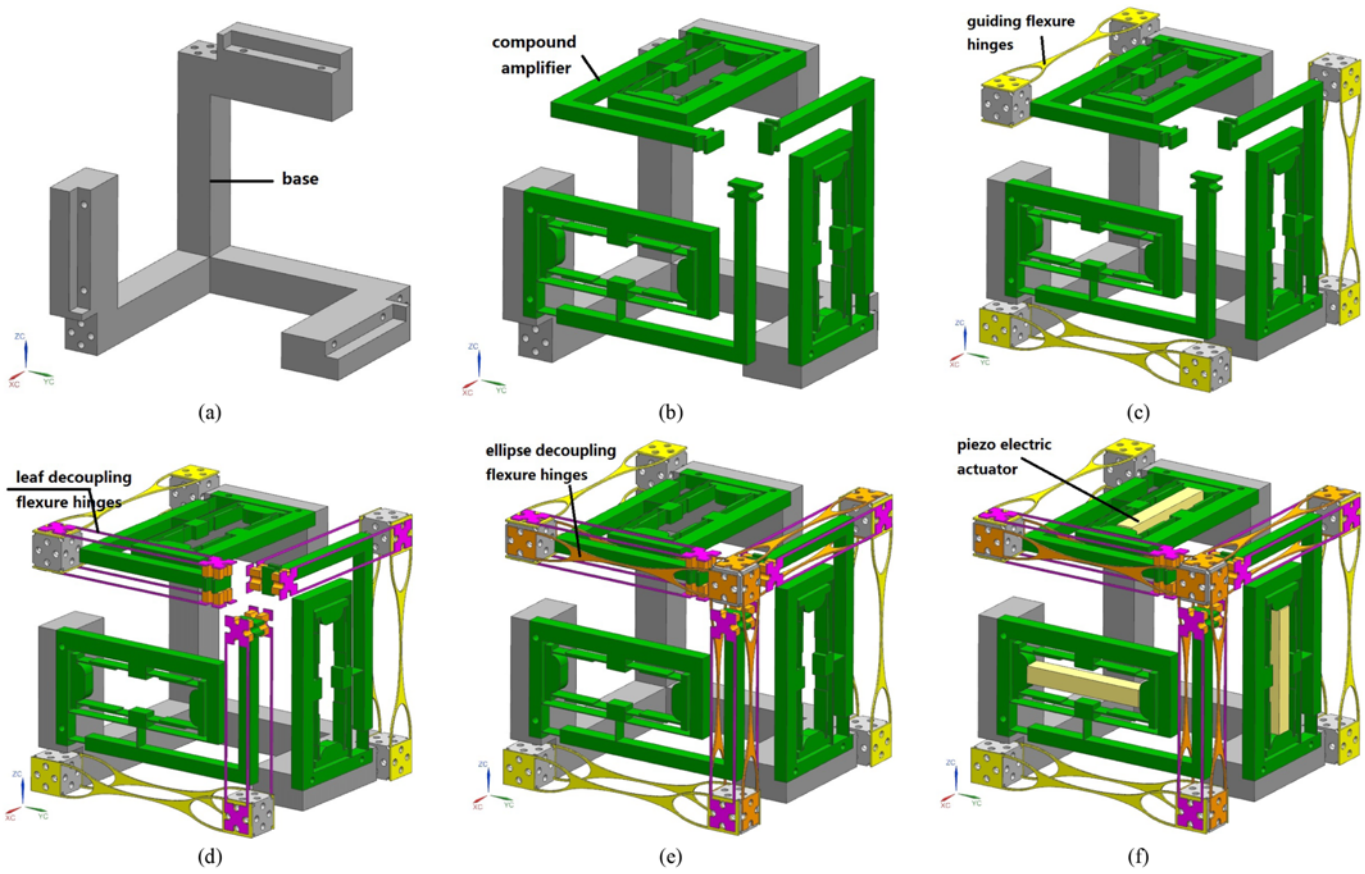

Fig. 2 Assembly process of the 3-DOF micropositioning stage; (a) Base, (b) compound amplifier, (c) guiding flexure hinges of type A, (d) leaf decoupling flexure hinges of type B, (e) ellipse-shaped decoupling flexure hinges of type A, and (f) piezoelectric actuator

between the modules of parallel joint and the amplifier.

It is notable that the simple elastic hinge leads to rotational motion, which is not desired for pure translational motion generation. The proposed complex form of elastic hinges can reduce the influence of rotational motion and enhance the loading capacity of the XYZ stage.

2.2 Assembly process

The overall positioning mechanism is assembled by combining all of the necessary components together. The assembly process is divided into six steps. As shown in Fig. 2(a), the first step prepares the fundamental base for the whole positioner. Then, three compound amplifier modules are added to the base, as shown in Fig. 2(b). Later, as depicted in Fig. 2(c), three parallel joints of type A are assembled to guide the path for the output motion. Next, the amplifier modules are connected to the guiding flexure hinges by three pairs of parallel assembled decoupling flexure hinges of type B, with details illustrated in Fig. 2(d). The decoupling flexure hinges of type A are then mounted to connect the platform with amplifier, as shown in Fig. 2(e). Finally, the piezoelectric actuators are installed in the amplifier modules as depicted in Fig. 2(f).

3. Analytical Modeling

In this section, the statics and dynamics models of the 3-DOF parallel positioning stage are derived analytically.

3.1 Model of the amplifier module

The compound amplifier is composed of the bridge-principle amplifier and lever-principle amplifier.

Based on the previous work for the elastic deformation of one quarter model for bridge-principle amplifier,[23] the amplification ratio can be generated as:

$$R_1 = \frac{6(t_1-t_2)(L_1+2L_2)^3}{t_2^2[(L_1+2L_2)^2+(t_1-t_2)^2]+6(t_1-t_2)^2(L_1+2L_2)^2} \quad (1)$$

As the value of $(L_1+2L_2)^2$ in the denominator of the above equation is far larger than $(t_1+t_2)^2$, and the PZT offers the travel in both sides, which means that the output is reduced by half, the amplification ratio of the bridge-principle amplifier can be simplified as the following equation.

$$R_2 = \frac{3(t_1-t_2)(L_1+2L_2)}{t_2^2+6(t_1-t_2)^2} \quad (2)$$

For the lever-principle amplifier, the amplification ratio can be derived as:

$$R_3 = \frac{L_3+L_4}{L_3} \quad (3)$$

As the compound amplifier is serial connected by aforementioned

amplifier. So, the total amplification ratio is governed by

$$R_4 = R_2 R_3 \tag{4}$$

Substituting Eqs. (2) and (3) into Eq. (4), the total amplification ratio can be derived as

$$R_4 = \frac{3(t_1-t_2)(L_1+2L_2)(L_3+L_4)}{L_3[t_2^2+6(t_1-t_2)^2]} \tag{5}$$

3.2 Model of the stage

The model of the stage can be simplified as the combination of the amplifier modules and non-amplifier modules. Only the amplifier modules affect the output motion for the stage. The analytical model for the output motion of the stage can be derived as:

$$D_a = R_4 q \tag{6}$$

where q denotes the output of the PZT. With an input displacement of 32 μm applied, the stage can produce the travel of 1.21 mm analytically.

3.3 Dynamics modeling

In consideration of the decoupled property of the parallel ellipse-shaped decoupling flexure hinges (type A), the XYZ parallel mechanism is capable of reducing the parasitic motion and obtaining pure directional motion along X, Y, and Z axes. For the convenience of analytical modeling, it is assumed that the positioner is totally decoupled. Based on this assumption, when the three PZT actuators produce the one-sided input displacements of $q = [q_1, q_2, q_3]^T$, the kinetic energy can be calculated as:

$$T = \left[m_1\left(\frac{5}{8}R_2^2+\frac{1}{2}\right)+m_2+\frac{m_3}{2}R_2^2+\frac{m_4R_2^2(L_3+L_4+L_5)}{8L_3} + \frac{m_5R_4^2(L_3+L_4)}{2L_3}+\frac{3}{4}m_6R_4^2+\frac{7}{2}m_7R_4^2 \right] q^2 \tag{7}$$

where the mass components are denoted in Fig. 3. In addition, m_6 represents the mass for parallel flexure hinges and m_7 is the mass of the output platform.

Referring to Fig. 3, taking into account the analysis of the compound parallelogram flexure, with b representing the thickness of the flexure, the rotational stiffness of one leaf flexure for the P joint in bridge-principle amplifier can be derived as:

$$K_r = \frac{Ebt_1^3t_2^3}{12(2l_2t_1^3+l_1t_2^3)} \tag{8}$$

where E is the Young's modulus of the material (Al-6061 in this work).

The rotational stiffness of the leaf flexure hinge in lever-principle amplifier is derived as:

$$K_p = \frac{Ebt_2^3}{12l_5} \tag{9}$$

For a pair of parallel ellipse-shaped flexure hinges (type A), the rotational stiffness of the flexure hinges is

$$K_t = \frac{E'ta_2^3}{6L_7 f} \tag{10}$$

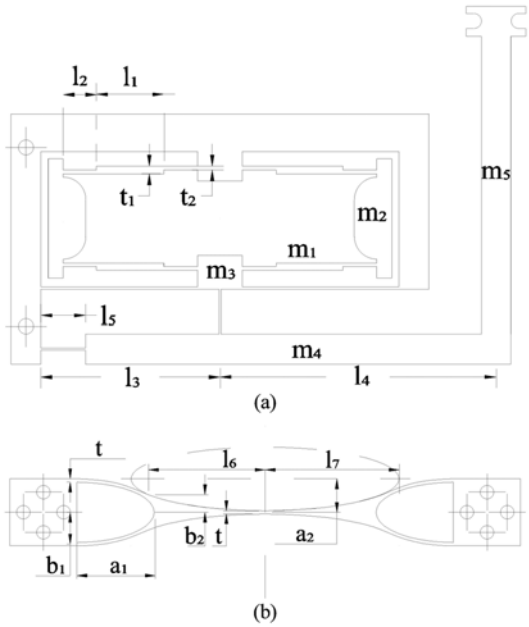

Fig. 3 Architectural parameters of (a) compound amplifier and (b) ellipse-shaped decoupling flexure hinges

where E' is the Young's modulus of the material ABS plus, and f can be derived as:

$$f = \int_{-\pi/2}^{\pi/2} \frac{\cos\gamma}{(t/a_2+2-\cos\gamma)} d_\gamma = \frac{12s^4(2s+1)arctan\sqrt{4s+1}}{(4s+1)^{5/2}} + \frac{2s^3(16s^2+4s+1)}{(2s+1)(4s+1)^2} \tag{11}$$

where $s = a_2/t$. The rotational stiffness for the leaf flexure hinges is calculated by

$$K_t' = \frac{E'f_b t^3}{6L_7} \tag{12}$$

where t denotes the thickness of the leaf flexure hinge and f_b can be derived as:

$$f_b = \int_0^{a_1-t}\left[b_1\sqrt{1-\frac{x^2}{a_1^2}}-(b_1-t)\sqrt{1-\frac{x^2}{(a_1-t)^2}} \right] + \int_{a_1-t}^{a_1} 2b_1\sqrt{1-\frac{x^2}{a_1^2}} + \int_{a_1}^{a_1+l_6} 2a_2\left(1-\sqrt{1-\frac{(x-a_2-l_6)^2}{L_7}}\right) \tag{13}$$

In addition, the potential energy is derived as follows.

$$V = 8\times\frac{1}{2}K_r\theta_1^2+\frac{1}{2}K_p\theta_2^2+4\times\frac{1}{2}K_t\theta_3^2+2\times\frac{1}{2}K_t'\theta_3^2 \tag{14}$$

where θ_1 and θ_2 are the rotational angles for leaf flexure hinge of the bridge-type amplifier and lever-principle amplifier, respectively, which can be approximatively solved by the following equations as the rotational angle is very small. In addition, θ_3 indicates the rotational angle for parallel flexure hinge and L_8 denotes the length of these hinges.

$$\theta_1 = \frac{qR_2}{2(L_1+2L_2)},\ \theta_2 = \frac{qR_2}{L_3},\ \theta_3 = \frac{qR_4}{L_8}.$$

The dynamics model of the positioner can be developed based on the Lagrange's equations:

$$\frac{d}{d_t}\left(\frac{\partial T}{\partial \dot{q}_i}\right)-\frac{\partial T}{\partial q_i}+\frac{\partial V}{\partial q_i}=F_i \tag{15}$$

To solve the resonant frequency of the positioner, the external force F_i is set as 0 N. Then, by combining Eqs. (7), (14), and (15), the dynamic model can be derived as

$$M\ddot{q}-K\dot{q}=0 \tag{16}$$

Then, the resonant frequency (in unit of Hertz) of the positioner in the working direction is derived as follows.

$$f=\frac{1}{2\pi}\sqrt{\frac{K}{M}} \tag{17}$$

with

$$M=m_1\left(\frac{5}{4}R_2^2+1\right)+2m_2+m_3R_2^2+\frac{m_4R_2^2(l_3+l_4+l_5)}{4l_3}+\frac{m_5R_4^2(l_3+l_4)}{l_3}+\frac{3m_6R_4^2}{2}+m_7R_4^2 \tag{18}$$

$$K=8K_r\theta_1^2+K_p\theta_2^2+4K_t\theta_3^2+2K_t'\theta_3^2 \tag{19}$$

where K and M in Eq. (16) are the diagonal matrices with elements K and M expressed by Eq. (19) and Eq. (18), respectively.

The resonant frequency along the working direction during translational motion is 79 Hz as calculated by Eq. (17).

4. FEA Simulation Study

In this section, the FEA simulation of the micropositioning stage is conducted using ANSYS software to verify the parameters for the stage and to reveal the performance of the stage. First, the optimization for the bridge-type amplifier is conducted to get a larger amplification ratio and the travel motion of the positioner is evaluated with static structural analysis simulation. Then, the fatigue analysis is carried out to test the durability of the stage. Finally, the resonant frequency is predicted with modal analysis.

The architectural parameters of the mechanism are illustrated in Figs. 3(a) and 3(b). These parameters are tabulated in Table 1, which are designed by trial and error to obtain the design objective of larger travel range for the micropositioning stage.

4.1 Model of the amplifier module

In this section, the optimization of bridge-type amplifier module is performed by conducting FEA simulation. The reference models are set as ideal situations in the previous section. In order to test the performance of the designed stage and to verify the accuracy of the established models, FEA simulations are conducted with ANSYS software package. For manufacturing, a plate of Al-6061 alloy material of 4 mm thickness is selected in this work. The key specification data of the material are: Young's modulus = 71 GPa, yield strength = 280 MPa, Poisson ratio = 0.33, and density = 2.77×10^3 kg/m^3. The input displacement is set as 32 μm, which is the maximum output of the PZT actuator (P-885.91).

Table 1 Parameters of the 3-DOF micropositioning stage

Parameters	L_1	Ll_2	L_3	L_4	L_5	L_6
Dimension (mm)	9.0	4.5	24.0	35.0	6.0	17.5
Parameters	L_7	L_8	t	t_1	t_2	-
Dimension (mm)	20	56.0	0.5	0.5	1.0	-

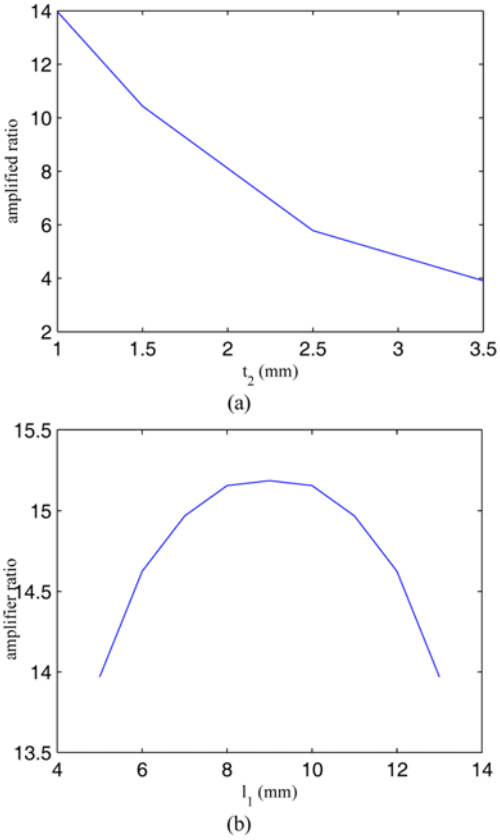

Fig. 4 Optimization process of parameters (a) t_2 and (b) l_1

Parameter t_1 is limited by the fabrication precision. The amplifier module of the stage is verified in terms of two essential parameters. One parameter is the thickness of leaf flexure for the bridge-type amplifier t_2, and the other one is the length l_1 for bridge-type amplifier. The range of t_1 is set as 1.0 mm $\leq t_1 \leq$3.5 mm to cater for the fabrication precision and compact overall size. Fig. 4 shows that with parameters t_2=0.5mm and l_1= 9mm, the bridge amplifier can obtain the largest amplification ratio of 15.2, with the output of 487 μm as shown in Fig. 5(a).

4.2 Static structural simulation

The testing of output motion along X, Y, and Z axes is demonstrated firstly in this part. With the PZT actuator located for Z-axis motion generation, it produces the output motion of 32 μm totally.

It is the maximum displacement that can be produced by the adopted actuator (model P-885.91 from PI GmbH).

The positioner can provide the average output displacement of 1.05 mm along Z-axis, which is 32.8 times the input as shown in FEA simulation result in Fig. 5(b). Due to the symmetry property for this positioner mechanism, the output motions along X and Y axes are the

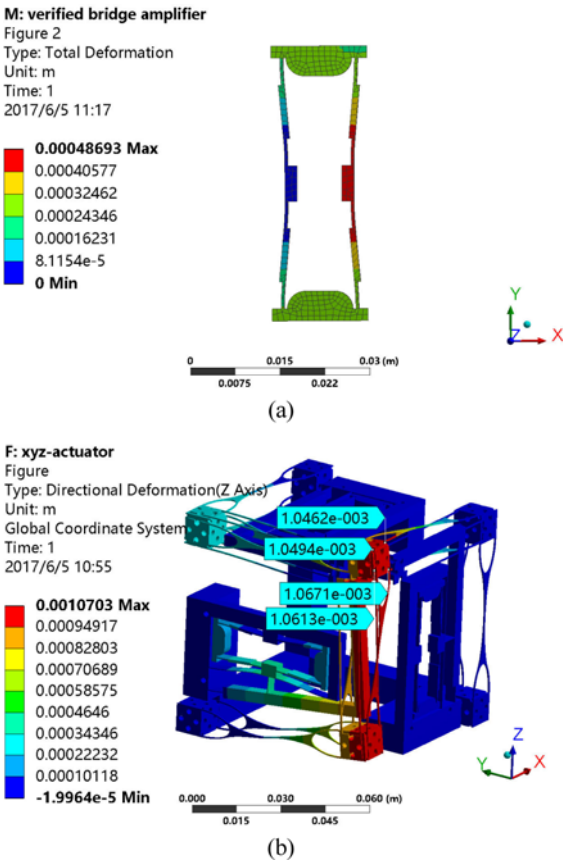

Fig. 5 FEA simulation results of (a) bridge-type amplifier module and (b) the whole stage

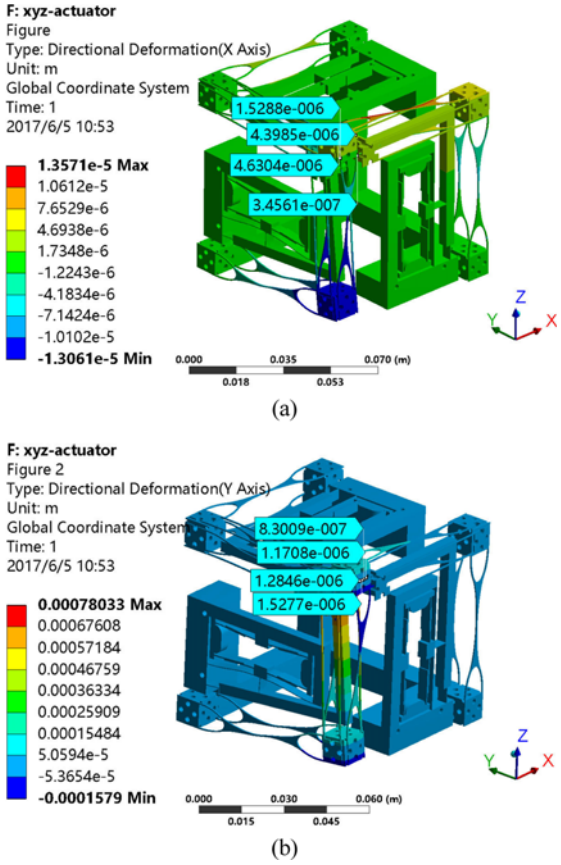

Fig. 6 Parasitic displacement results. (a) Cross-axis motion along X axis, (b) cross-axis motion along Y axis

Table 2 Simulation results of decoupling property testing

Axes	X	Y	Z
Input (μm)	-	-	32
Output (μm)	2.70	1.25	1050
Cross-axis motion (%)	0.26	0.12	-

same to that in the Z axis.

The analytical result for the output of positioner is 1.21 mm, which is 13.5% larger than FEA simulation result. The deviation between the analytical result and FEA simulation is induced because the ideal model is used in analytical process.

Then, the decoupling analysis of the positioner is conducted. When the positioner is actuated to translate in Z-axis as shown in Fig. 5(b), the average cross-axis errors are 2.7 μm along X axis and 1.25 μm along Y axis, as shown in Figs. 6(a) and 6(b). The percentage of cross-axis errors along X and Y axes are only 0.26% and 0.12%, respectively, which indicate that the motion along Z axis is almost decoupled from the X axis and Y axis. Similar to the analysis of travel range testing, the decoupling motion analysis along X, Y, and Z axes can be conducted independently. Table 2 shows the decoupling property of the positioner.

4.3 Stress analysis

Stress analysis is conducted to evaluate the material's capability for the designed micropositioning stage. As shown in Fig. 7, the equivalent

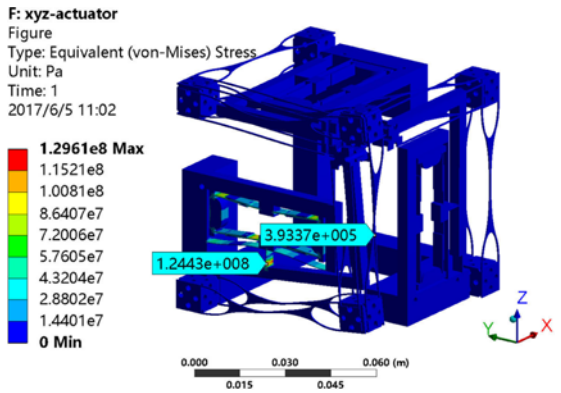

Fig. 7 Simulation result of equivalent alternating stress distribution

alternative stress of the amplifier module is 124 MPa, which is much lower than the yield stress (275 MPa) of the material Al-6061. The equivalent alternative stress for flexure hinges with the material of ABS Plus for 3D printer is only 0.39 MPa, which is also lower than the yield stress (31 MPa) of the used material. So, the positioner can work normally.

4.4 Modal analysis

The dynamic performance of the positioning mechanism is evaluated by conducting modal analysis. As shown in Figs. 8(a), 8(b),

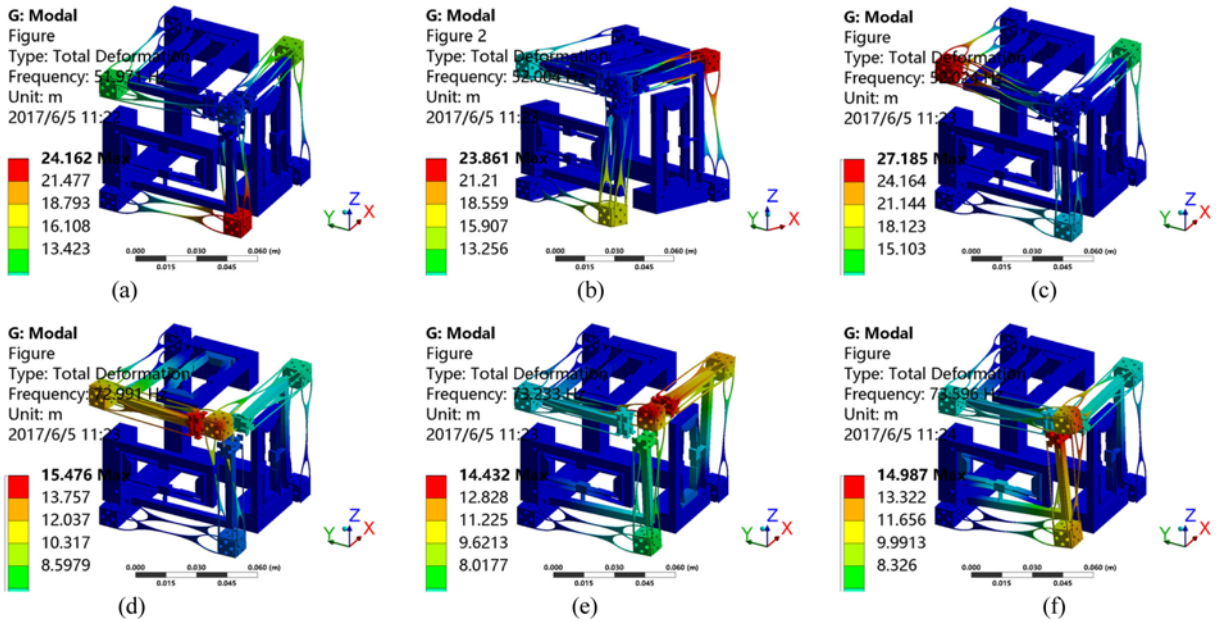

Fig. 8 Simulation results of first-six resonant modes of the 3-DOF micropositioning mechanism

and 8(c), the first-order resonant frequencies of the stage are 51.97 Hz, 52.00 Hz, and 52.02 Hz. The second-order resonant frequencies appear at 72.99 Hz, 73.23 Hz, and 73.60 Hz, respectively. The first three resonant modes denote the rotational motion along the three axes, while the latter three resonant modes represent the translation along each axis. It is notable that a higher resonant frequency of the stage structure can be generated by increasing the stiffness and reducing the mass of moving components of the mechanism.

The dynamics model predicts that the resonant frequencies along the three working direction are all equal to 79.15 Hz. As compared with the FEA simulation result of average 73 Hz in the travel direction, the analytical model result is 25.3% larger. The discrepancy is mainly caused by the assumption adopted in the analytical model, which considers connecting links as rigid bodies. By contrast, every deformation has been considered in the FEA simulation. Hence, simulation result is more accurate than analytical model result.

In addition, it is observed that the rotation mode has a smaller resonance frequency than the linear mode. Generally, the vibration mode in the desired direction should be at least twice as small as other modes to have a robust mechanism. In this work, considering that the targeted application of the XYZ stage is micromanipulation such as biological cell microinjection, the operating frequency is usually lower than 10 Hz. Hence, the designed stage will work stably for such kind of low-frequency applications. In the future work, a more robust mechanism will be explored to improve the dynamics performance of the XYZ stage.

5. Prototype Fabrication and Open-loop Testing

To test the performance of the stage, a prototype is fabricated by using multiple types of materials, and open-loop testing is conducted on the prototype by experimental study.

5.1 Prototype fabrication

The aluminum alloy Al-6061 is selected as the material of amplifier module owing to its good elastic property. It can generate larger deformation in elastic regime along with lower cost than other metals under the identical size and shape. It also can transmit the large output force of the PZT actuator.

The amplifier module is manufactured by wire-electric discharging machining (EDM) with high precision of 0.03 mm. To reduce the mass of moving components, the decoupling flexure hinges are fabricated with the material of acrylonitrile butadiene styrene plus (ABS plus) using a 3D printer (model: uPrint SE Plus, from Stratasys Ltd.). The parallel flexure joints can be easily produced by the 3D printer. As compared with other traditional manufacturing process, 3D printer can save much time and effort in fabrication. The minimum feature size of 3D printer is 1.0 mm × 0.25 mm, which means that the thickness of the flexure needs to be larger than 0.25 mm and the width needs to be no less than 1.0 mm.

The prototype is depicted in Fig. 9. It possesses a compact dimension of 77 mm × 77 mm × 77 mm.

5.2 Statics performance testing results

The open-loop test is conducted to verify the performance of the prototype. As shown in Fig. 9, a linear voltage amplifier is applied to obtain enlarged voltage for driving the PZT actuator. Laser sensors are used to measure the displacement of the designed stage. NI instrument can transfer the input and output date to computer to realize the open-loop control of the stage prototype.

As only two probes are available and the data of three axes need to be collected, the data are collected in two steps. The data for X axis and Y axis is obtained in first step as shown in Fig. 9(a), where two probes are arranged in XY plane. Then, the data along Z axis are collected by a probe arranged in Z axis as shown in Fig. 9(b). The input is set as sinusoidal waveform with magnitude ranging from 0 to 10 V. Then, the

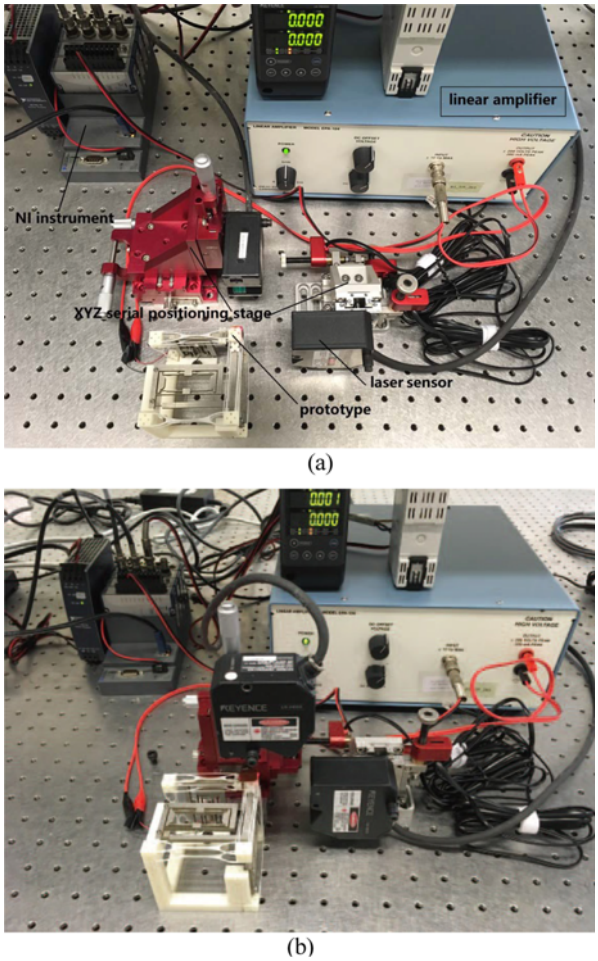

Fig. 9 Experimental setup of the prototype: (a) Setup 1, (b) setup 2

Table 3 Comparison of the motion range and decoupling rate of typical works

Works	Input (μm)	Output (μm)	Coupling (%)
Ref. 27	20	141	7.1
Ref. 28	20	164.8	4.5
X-axis in this work	32	582	3.4
Y-axis in this work	32	517	4.8
Z-axis in this work	32	524	2.8

linear amplifier gives a ten-times enlarged voltage to drive the PZT. With the driving voltage from 0 to 100 V, the PZT offers a translational motion from 0 μm to 32 μm. The amplifier module and decoupling flexure hinges transfer the motion to the platform. Finally, the output displacement of the stage is measured by the laser sensors.

The relationships between the displacements and driving voltages for X, Y, and Z axes are shown in Fig. 10(a), (b) and (c), which illustrate the stage output property with the open-loop voltage-driven strategy. For each axis, the relationship between the stage output displacement and input voltage of PZT is nonlinear as indicated by the hysteresis loop. For Y axis and Z axis, the data show the similar result because the stage is of central symmetry. The strokes of the output along X, Y, and Z axes are 582 μm, 517 μm, and 524 μm, respectively. The difference of the output is caused by the different preloading

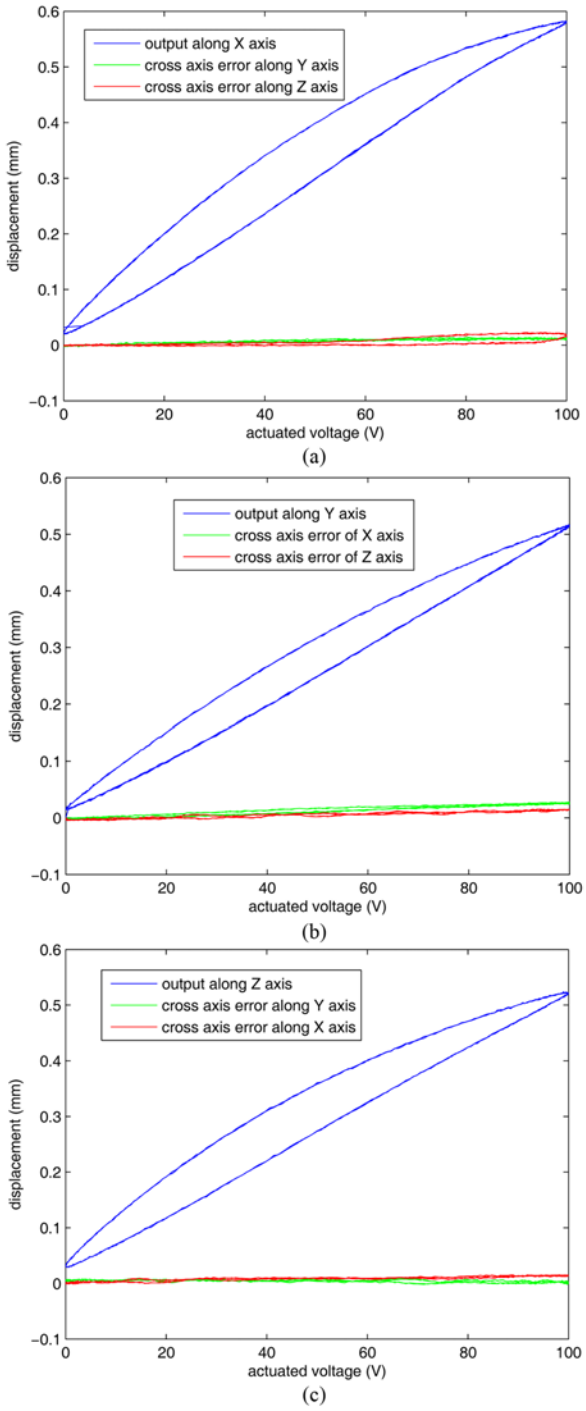

Fig. 10 Experimental testing results of output motion along (a) X axis, (b) Y axis, and (c) Z axis

effects for PZT actuators. The average deviation caused by the cross-axis motion for X, Y, and Z axes are 20 μm, 25 μm, and 15 μm, which are around 3.4%, 4.8%, and 2.8% of the total ranges, respectively. The derivation is acceptable and the difference of the deviation towards three axes is attributed to the manufacturing and assembly errors.

Table 3 shows a comparison for the motion range and percentage of the decoupling of the proposed 3-DOF stage versus existing works. It indicates that the proposed stage can obtain larger workspace and better decoupling performance than existing work.[27,28]

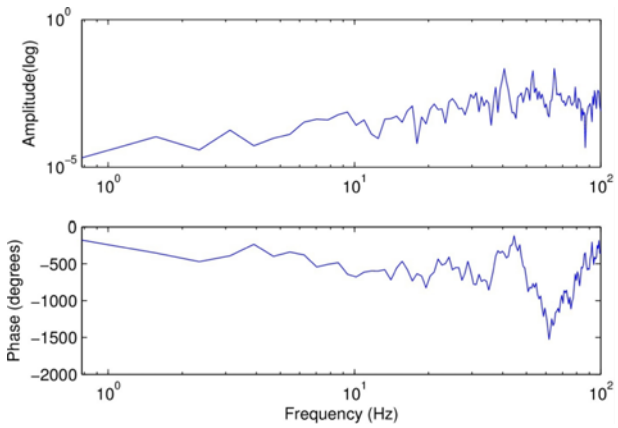

Fig. 11 Experimental testing results of frequency response

In addition, the discrepancy between the simulation and experimental results for the output displacement is caused by the lost motion during the transmission in the flexure mechanism.

5.3 Dynamics performance testing results

The frequency response is tested by applying a sine waveform voltage with the magnitude of 0 to 1.0 V and frequency up to 200 Hz. The frequency response is shown in the Bode plots in Fig. 11. It is observed that the amplitude plot exhibits some fluctuations, which may be caused by the relatively low stiffness of the fabricated prototype. Ignoring the interference of unknown factor, the peak value and the big decrease of the phase angle indicates the response frequency of the stage reaches its first resonant frequency. It is seen that the first dominant resonant frequency along the working direction occurs around 69 Hz.

In addition, Table 4 indicates that the FEA simulation result is very close to the experimental result with 5.8% deviation. The discrepancy between the analytical and experiment results is 14.5%, which is induced by the fact that simplification is adopted in analytical modeling process.

5.4 Further discussion

Driven by piezoelectric actuators with stroke of 32 μm, experimental results reveal the output displacement of 580 μm. For the purpose of comparison, the travel ranges in each axis of the XYZ stage evaluated by different approaches are summarized in Table 5. It is seen that there is a relatively large difference between the model and experimental results. The main reason arises from the fabrication error of the stage parameters. Analytical model is more efficient for an optimization design of the stage structure. Actually, the model results can be improved by multiplying a correction factor.

In addition, the discrepancy between simulation and experimental results is attributed to the guiding flexure hinges between the amplifier module and platform, which consumes the output motion from the amplifier module. In addition, the connection for decoupling flexure modular and guiding flexure modular is realized by cyanoacrylate adhesives which lead to a reduction on the output motion. Nevertheless, the stage achieves a large displacement amplification ratio of 18.2 as evaluated by open-loop experimental testing.

Table 4 Comparison of the resonant frequency of the stage

Approach	Resonant frequency (Hz)	Deviation (%)
Analytical	79	14.5
FEA	73	5.8
Experiment	69	-

Table 5 Comparison of the travel ranges obtained by different approaches

Approach	Travel range (mm)	Deviation (%)
Analytical	1.21	108.6
FEA	1.05	81.0
Experiment	0.58	-

6. Conclusion

This paper reports a novel XYZ micropositioning stage with compound displacement amplifier and parallel flexure hinges. The statics and dynamics models are derived in analytical forms and verified by conducting FEA simulation studies. The positioner mechanism exhibits a compact dimension within 77 mm × 77 mm × 77 mm. The stage can provide a nearly decoupled translational motion along X, Y, and Z. A prototype is fabricated for experimental testing. The output displacement is larger than that in existing recent works of 3-DOF parallel positioning mechanisms. The improvement on output displacement of the stage extends the application for micro-scale operation. The dynamic performance of the mechanism has also been evaluated. Results show that the first resonant frequency of the micropositioning stage is up to 69 Hz in working direction. The developed 3-DOF micropositioning stage can be applied in various applications, e.g., biological cell microinjection. In the future work, closed-loop control will be implemented to realize a precision positioning control for the micropositioning stage, and the proposed stage can be applied in 3D microinjection operation.

ACKNOWLEDGEMENT

The work was support by the National Natural Science Foundation of China under Grant No. 51575545, and the Macao Science and Technology Development Fund under Grant No. 090/2015/A3 and 143/2016/A.

REFERENCES

1. Escande, C., Chettibi, T., Merzouki, R., Coelen, V., and Pathak, P. M., “Kinematic Calibration of a Multisection Bionic Manipulator,” IEEE/ASME Transactions on Mechatronics, Vol. 20, No. 2, pp. 663-674, 2015.
2. Zhuang, H., Wu, W.-C., and Roth, Z. S., “Camera-Assisted Calibration of SCARA Arms,” Proc. of IEEE/RSJ International Conference on Intelligent Robots and Systems, pp. 507-512, 1995.
3. Pierrot, F., Nabat, V., Company, O., Krut, S., and Poignet, P., “Optimal Design of a 4-DOF Parallel Manipulator: From Academia

to Industry," IEEE Transactions on Robotics, Vol. 25, No. 2, pp. 213-224, 2009.

4. Gozen, B. A. and Ozdoganlar, O. B., "Design and Evaluation of a Mechanical Nanomanufacturing System for Nanomilling," Precision Engineering, Vol. 36, No. 1, pp. 19-30, 2012.
5. Tian, Y., Shirinzadeh, B., and Zhang, D., "Design and Dynamics of a 3-DOF Flexure-Based Parallel Mechanism for Micro/Nano Manipulation," Microelectronic Engineering, Vol. 87, No. 2, pp. 230-241, 2010.
6. Beyeler, F., Neild, A., Oberti, S., Bell, D. J., Sun, Y., et al., "Monolithically Fabricated Microgripper with Integrated Force Sensor for Manipulating Microobjects and Biological Cells Aligned in an Ultrasonic Field," Journal of Microelectromechanical Systems, Vol. 16, No. 1, pp. 7-15, 2007.
7. Xu, Q., "Output-Based Discrete-Time Sliding Mode Control for a Piezoelectrically Actuated System," Nonlinear Dynamics, Vol. 76, No. 1, pp. 551-559, 2014.
8. Bhagat, U., Shirinzadeh, B., Clark, L., Qin, Y., Tian, Y., and Zhang, D., "Experimental Investigation of Robust Motion Tracking Control for a 2-DOF Flexure-Based Mechanism," IEEE/ASME Transactions on Mechatronics, Vol. 19, No. 6, pp. 1737-1745, 2014.
9. Pokines, B. J. and Garcia, E., "A Smart Material Microamplification Mechanism Fabricated Using LIGA," Smart Materials and Structures, Vol. 7, No. 1, pp. 105-112, 1998.
10. Ma, H.-W., Yao, S.-M., Wang, L.-Q., and Zhong, Z., "Analysis of the Displacement Amplification Ratio of Bridge-Type Flexure Hinge," Sensors and Actuators A: Physical, Vol. 132, No. 2, pp. 730-736, 2006.
11. Xu, Q. and Li, Y., "Design of a New Decoupled XYZ Compliant Parallel Micropositioning Stage with Compact Structure," Proc. of IEEE International Conference on Robotics and Biomimetics (ROBIO), pp. 901-906, 2009.
12. Qi, K.-Q., Xiang, Y., Fang, C., Zhang, Y., and Yu, C.-S., "Analysis of the Displacement Amplification Ratio of Bridge-Type Mechanism," Mechanism and Machine Theory, Vol. 87, pp. 45-56, 2015.
13. Chen, G., Ma, Y., and Li, J., "A Tensural Displacement Amplifier Employing Elliptic-Arc Flexure Hinges," Sensors and Actuators A: Physical, Vol. 247, pp. 307-315, 2016.
14. Ling, M., Cao, J., Jiang, Z., and Lin, J., "Theoretical Modeling of Attenuated Displacement Amplification for Multistage Compliant Mechanism and Its Application," Sensors and Actuators A: Physical, Vol. 249, pp. 15-22, 2016.
15. Wadikhaye, S. P., Yong, Y. K., Bhikkaji, B., and Moheimani, S. R., "Control of a Piezoelectrically Actuated High-Speed Serial-Kinematic AFM Nanopositioner," Smart Materials and Structures, Vol. 23, No. 2, Paper No. 025030, 2014.
16. Xu, Q., "New Flexure Parallel-Kinematic Micropositioning System with Large Workspace," IEEE Transactions on Robotics, Vol. 28, No. 2, pp. 478-491, 2012.
17. Qin, Y., Shirinzadeh, B., Tian, Y., Zhang, D., and Bhagat, U., "Design and Computational Optimization of a Decoupled 2-DOF Monolithic Mechanism," IEEE/ASME Transactions on Mechatronics, Vol. 19, No. 3, pp. 872-881, 2014.
18. Kim, H. and Gweon, D.-G., "Development of a Compact and Long Range XYθz Nano-Positioning Stage," Review of Scientific Instruments, Vol. 83, No. 8, Paper No. 085102, 2012.
19. Choi, K.-B., Lim, H. J., Kim, G. H., and Lee, J. J., "A Flexure-Based Scanner for a Fully Bidirectional Operation Driven by a Differential Piezo Force," Proc. of the Institution of Mechanical Engineers, Part C: Journal of Mechanical Engineering Science, Vol. 228, No. 17, pp. 3186-3199, 2014.
20. Lobontiu, N., "Modeling and Design of Planar Parallel-Connection Flexible Hinges for In- and Out-of-Plane Mechanism Applications," Precision Engineering, Vol. 42, pp. 113-132, 2015.
21. Liu, P.-B., Yan, P., Zhang, Z., and Leng, T.-T., "Flexure-Hinges Guided Nano-Stage for Precision Manipulations: Design, Modeling and Control," Int. J. Precis. Eng. Manuf., Vol. 16, No. 11, pp. 2245-2254, 2015.
22. Huang, S.-C. and Dao, T.-P., "Design and Computational Optimization of a Flexure-Based XY Positioning Platform Using FEA-Based Response Surface Methodology," Int. J. Precis. Eng. Manuf., Vol. 17, No. 8, pp. 1035-1048, 2016.
23. Zhang, X., Zhang, Y., and Xu, Q., "Design and Control of a Novel Piezo-Driven XY Parallel Nanopositioning Stage," Microsystem Technologies, Vol. 23, No. 4, pp. 1067-1080, 2017.
24. Liu, Y. and Xu, Q., "Design of a Flexure-Based Auto-Focusing Device for a Microscope," Int. J. Precis. Eng. Manuf., Vol. 16, No. 11, pp. 2271-2279, 2015.
25. Ruiz, A., Campa, F., Roldán-Paraponiaris, C., Altuzarra, O., and Pinto, C., "Experimental Validation of the Kinematic Design of 3-PRS Compliant Parallel Mechanisms," Mechatronics, Vol. 39, pp. 77-88, 2016.
26. Guo, K., Ni, M., Chen, H., and Sui, Y., "A Monolithic Adjusting Mechanism for Optical Element Based on Modified 6-PSS Parallel Mechanism," Sensors and Actuators A: Physical, Vol. 251, pp. 1-9, 2016.
27. Li, Y. and Xu, Q., "Design and Optimization of an XYZ Parallel Micromanipulator with Flexure Hinges," Journal of Intelligent & Robotic Systems, Vol. 55, No. 4, pp. 377-402, 2009.
28. Xu, Q. and Li, Y., "Optimal Design and Fabrication of a Piezoactuated Flexure XYZ Parallel Micropositioning Stage," Proc. of IEEE/RSJ International Conference on Intelligent Robots and Systems (IROS), pp. 3682-3687, 2010.
29. Hao, G. and Li, H., "Design of 3-Legged XYZ Compliant Parallel Manipulators with Minimised Parasitic Rotations," Robotica, Vol. 33, No. 4, pp. 787-806, 2015.